Lab on a Chip

A Facile Multi-Material Direct Laser Writing Strategy

Journal:	*Lab on a Chip*
Manuscript ID	LC-COM-04-2019-000398.R1
Article Type:	Communication
Date Submitted by the Author:	02-Jun-2019
Complete List of Authors:	Lamont, Andrew; University of Maryland at College Park, Department of Mechanical Engineering; University of Maryland at College Park, Fischell Department of Bioengineering; University of Maryland at College Park, Robert E. Fischell Institute for Biomedical Devices Restaino, Michael; University of Maryland at College Park, Department of Mechanical Engineering; University of Maryland at College Park, Fischell Department of Bioengineering; University of Maryland at College Park, Robert E. Fischell Institute for Biomedical Devices Kim, Matthew; University of Maryland at College Park, Department of Mechanical Engineering; University of Maryland at College Park, Fischell Department of Bioengineering; University of Maryland at College Park, Robert E. Fischell Institute for Biomedical Devices Sochol, Ryan; University of Maryland at College Park, Department of Mechanical Engineering; University of Maryland at College Park, Fischell Department of Bioengineering; University of Maryland at College Park, Robert E. Fischell Institute for Biomedical Devices

Lab on a Chip

Communication

Cite this: DOI: 10.1039/xxxxxxxxxx

A Facile Multi-Material Direct Laser Writing Strategy†

Andrew C. Lamont,*[a] Michael A. Restaino,[a] Matthew J. Kim [a] and Ryan D. Sochol[a]

Received Date
Accepted Date

DOI: 10.1039/xxxxxxxxxx

www.rsc.org/journalname

Direct Laser Writing (DLW) is a three-dimensional (3D) manufacturing technology that offers vast architectural control at submicron scales, yet remains limited in cases that demand microstructures comprising more than one material. Here we present an accessible microfluidic multi-material DLW (μFMM-DLW) strategy that enables 3D nanostructured components to be printed with average material registration accuracies of 100±70 nm (ΔX) and 190±170 nm (ΔY) – a significant improvement *versus* conventional multi-material DLW methods. Results for printing 3D microstructures with up to five materials suggest that μFMM-DLW can be utilized in applications that demand geometrically complex, multi-material microsystems, such as for photonics, meta-materials, and 3D cell biology.

A wide range of emerging applications in fields including optics and photonics,[1–3] optical and mechanical meta-materials,[4,5] and biomedicine[6,7] rely on the unparalleled micro/nanoscale geometric versatility enabled by DLW. DLW-based manufacturing involves the use of a tightly focused femtosecond pulsed IR laser to initiate photopolymerization *via* two-photon (or multi-photon) absorption phenomena at designed locations within a liquid-phase photoreactive material.[8,9] By positioning the laser focal point or "voxel" in a point-by-point and/or layer-by-layer manner, 3D structures comprised of cured photomaterial can be additively manufactured with resolutions on the order of 100 nm.[10,11] Similar to many photopolymerization-based additive manufacturing technologies, such as stereolithography[12,13], continuous liquid interface production,[14] and computed axial lithography,[15] a challenge for DLW is the fabrication of printed structures comprised of two or more fully integrated photomaterials.[16]

Previously, several groups have demonstrated that DLW can be employed to print multi-material systems in which each material corresponds to distinct chemical, biological, and/or optical properties. In particular, Klein *et al.* reported the first multi-material DLW protocol to fabricate 3D cellular scaffolds with two materials (to either promote or inhibit cellular attachments).[17] Researchers have since extended this approach to print additional two-material 3D microarchitectures, including cellular environments,[18,19] composite meta-materials,[20,21] and optical components.[22,23] "Conventional" two-material DLW protocols consist of five primary steps: (*i*) drop casting a liquid-phase photomaterial onto a glass substrate, which is then loaded into a DLW printer, (*ii*) DLW of material-specific structures, after which the substrate is removed from the printer, (*iii*) performing material-specific development, (*iv*) repeating the first step with a different photomaterial, and then manually aligning the printing area to the previously fabricated structures to support rotational (θ) as well as X-, Y-, and Z-directional registration, and lastly (*v*) repeating steps (*ii*)-(*iii*) (*see also* **ESI Fig. S1**†; **ESI Text**†).[17] Although these steps can be repeated to integrate higher numbers of photomaterials, such approaches have never been demonstrated for the fabrication of structures with more than three materials.[24–27]

Despite the aforementioned advancements, conventional methods of multi-material DLW suffer from inherent limitations that have motivated the DLW community to generally avoid applications that rely on multi-material prints.[28] Although one drawback is that multi-material DLW protocols are significantly more time and labor-intensive than those required for single-material prints, the fundamental issues stem from the manual alignment step. Specifically, for each additional material, the registration accuracy is limited by the skill of the DLW printer operator. As a result, not only do multi-material systems need to be designed with extraneous alignment structures and/or tolerances that account for human error, but also, variations in user performance can diminish print-to-print repeatability and lead to higher rates of print failure compared to single-material runs. Recently, both we[29] and other groups[30] have posited that microfluidic devices can be leveraged to overcome these limitations. In particular,

[a] *Department of Mechanical Engineering, Fischell Department of Bioengineering, and Robert E. Fischell Institute for Biomedical Devices, 2152 Glenn L. Martin Hall, University of Maryland, College Park, Maryland, 20740, USA; Tel: (301)405-6928; E-mail: rsochol@umd.edu*

† Electronic Supplementary Information (ESI) available: Text and figures for 3D model preparation, conventional multi-material DLW, channel mold fabrication, and fabrication time; Movies of fabrication results for both μFMM-DLW and conventional multi-material DLW. See DOI: 10.1039/b000000x/

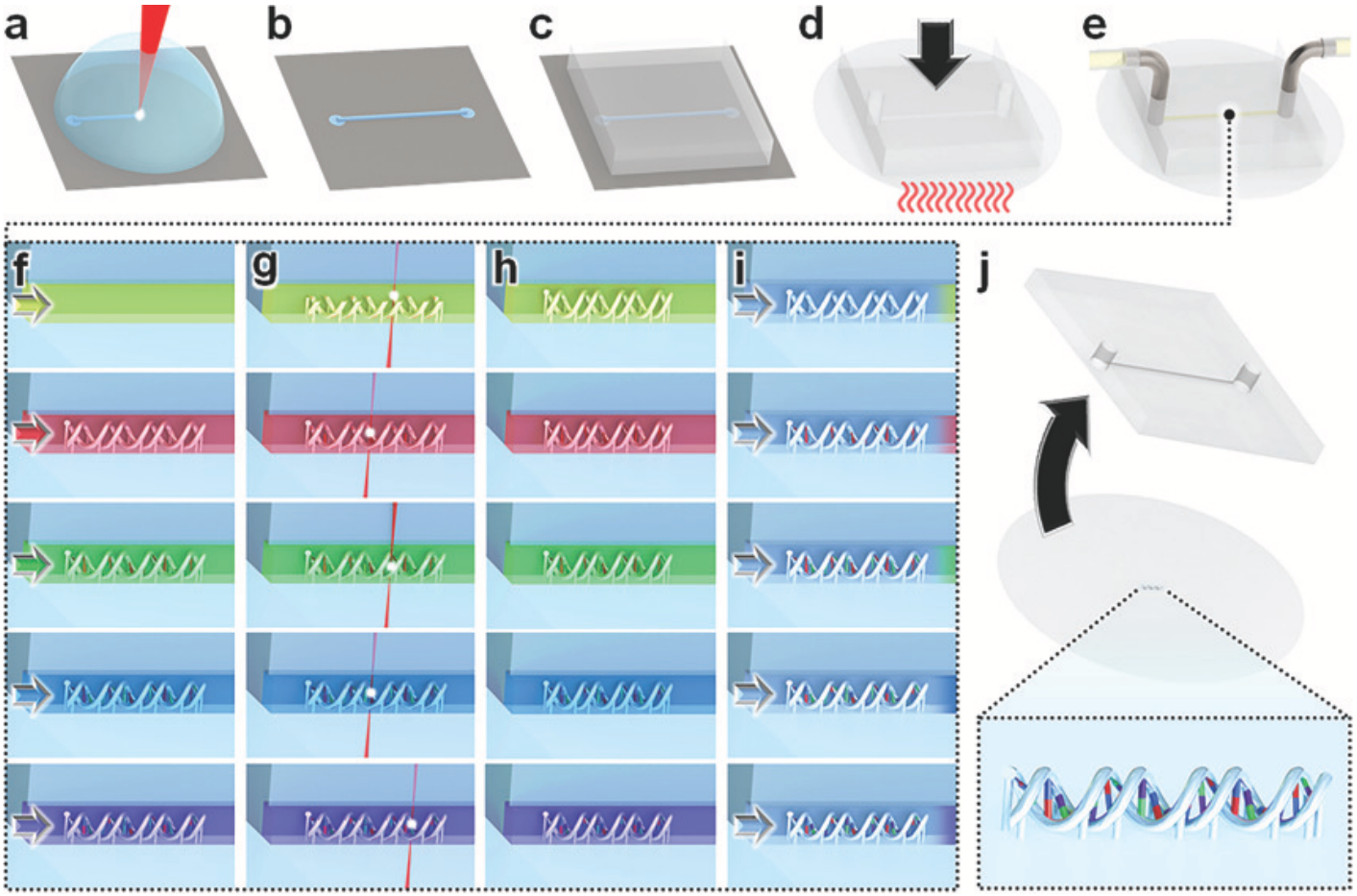

Fig. 1 Microfluidic multi-material direct laser writing (μFMM-DLW) concept. (**a**) DLW of negative channel mold structures. (**b**) Fully fabricated and post-processed channel negative master mold. (**c**) Micromolding of the negative master with polydimethylsiloxane (PDMS). (**d**) Thermal bonding of the processed PDMS layer to a circular glass substrate. (**e**) Connection of fluidic coupling and tubing to the channel. (**f-i**) Repeatable multi-material DLW procedure. (**f**) Vacuum-based perfusion of liquid-phase photocurable material into the microchannel to the fabrication site. (**g**) DLW of material-specific structures directly inside of the microchannel. (**h**) Completion of material-specific DLW fabrication. (**i**) Vacuum-based perfusion of liquid-phase developers. (**j**) Manual removal of PDMS following fabrication, leaving the completed print on the surface of the glass substrate.

Mayer *et al.* generated a stainless steel substrate mounting component for their DLW printer to produce a microfluidic channel connected to customized pressure-flow control units to deliver desired fluids (*e.g.*, distinct photomaterials and developers) to the DLW printing area.[30] In addition to challenges associated with the required metal manufacturing and electronics expertise, however, such approaches are poorly suited for cases that demand *in-situ* DLW (*is*DLW)[31,32] of multi-material 3D microstructures. To bypass these issues, here we present a μFMM-DLW strategy that leverages the accessibility of polydimethylsiloxane (PDMS) processing and an impermanent PDMS-to-glass thermal bonding technique to enable high multi-material registration accuracy, yet low fabrication time, cost, and labor (**Fig. 1**).

The μFMM-DLW approach in this work combines PDMS micromolding, impermanent PDMS-to-glass bonding, vacuum-based microfluidic infusion, and *is*DLW techniques[32] to realize 3D multi-material microstructure printing (**Fig. 1**). First, a negative master mold of a straight microchannel (100 μm $\times$ 100 μm cross section) was printed onto a Si substrate using the photoresist, IP-Dip (Nanoscribe GmbH, Germany), and the Nanoscribe Photonic Professional GT DLW printer in the Dip-in laser lithography (DiLL) configuration (**Fig. 1a**; *see also* **ESI Fig. S2**†; **ESI Text**†). The mold was then developed in successive washes of propylene glycol monomethyl ether acetate (PGMEA) for 15 min and isopropyl alcohol (IPA) for 2 min (**Fig. 1b**). A 10:1 (base:curing agent) mixture of PDMS (Sylgard 184, Dow, Midland, MI, USA) was cast over the negative master mold and thermally cured at 65 °C for 3 hrs (**Fig. 1c**). After removing the molded PDMS and punching holes at inlet and outlet locations, the PDMS was thermally (*i.e.*, weakly) bonded to a borosilicate glass substrate (30 mm diameter) under a 45 N load at 80 °C for 3 hrs (**Fig. 1d**).

In preparation for the *is*DLW printing process, solvent-resistant fluorinated ethylene propylene tubing (Cole Parmer, Vernon Hills, IL, USA) connected to stainless steel catheter couplers (Instech, Plymouth Meeting, PA, USA) were inserted into the inlet and outlet ports, allowing for vacuum pressure to be applied at the outlet, and in turn, fluidic infusion of desired photomaterials and developers into the microchannel *via* the inlet tubing (**Fig. 1e**). Specifically, the microdevice (with connected tubing) was loaded into the DLW printer in the oil-immersion configuration, and then multi-material microstructures were fabricated through the repetition of three fundamental steps: (*i*)approximately 100

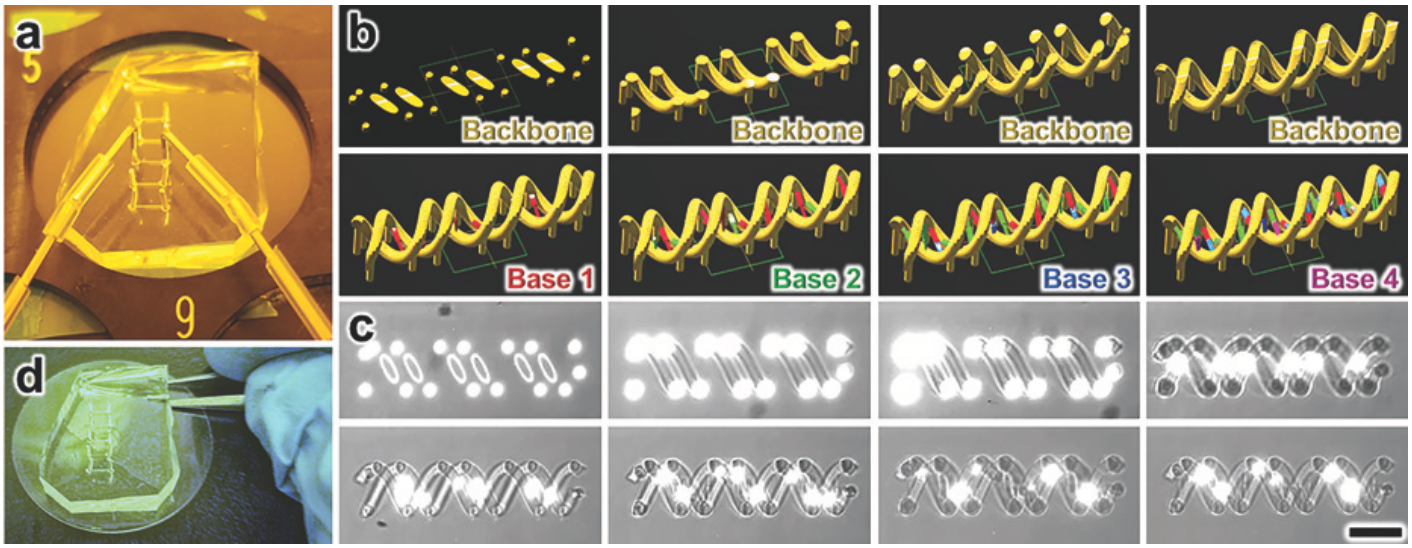

Fig. 2 Results for the μFMM-DLW fabrication process for a five-material DNA-inspired microstructure. (**a**) The mounted microfluidic device with fluidic tubing connected to inlet and outlet ports. (**b,c**) Computer-aided manufacturing (CAM) simulations (**b**) and corresponding micrographs (**c**) of μFMM-DLW fabrication (*see also* **ESI Movie 1**†). (**d**) Manual removal of PDMS layer with forceps following fabrication. Scale bar = 10 μm

μL of a photomaterial of interest was perfused through the tubing into the microchannel under an applied vacuum pressure (**Fig. 1f**); (*ii*) after discontinuing the vacuum pressure, microstructures corresponding to the loaded photomaterial were printed directly inside of the microchannel *via* an *is*DLW process in which the laser passes from a 63× objective lens, through an immersion oil, through the glass substrate, and then into the photomaterial (**Fig. 1g,h**); and (*iii*) developing solutions of PGMEA and IPA (5 and 2 mL respectively) were perfused into the microchannel under vacuum pressure for 5 min and 2 min, respectively, after which all remaining uncured photomaterial was visibly removed from the device (**Fig. 1i**). Upon completion of the μFMM-DLW process, the weak PDMS-to-glass bond allowed for the PDMS to be removed from the glass substrate, leaving behind the fabricated multi-material component on the unenclosed glass surface (**Fig. 1j**).

We utilized the μFMM-DLW approach to manufacture a five-material DNA-inspired microstructure inside of impermanently bonded PDMS-on-glass microfluidic channels (**Fig. 2a**). Results for computer-aided manufacturing (CAM) simulations and corresponding fabrication micrographs of the μFMM-DLW process are presented in **Figure 2b** and **c**, respectively, and **ESI Movie 1**†. This structure comprised five distinct material sections, including: (*i*) IP-Dip photoresist for the helical backbone, (*ii*) Rhodamine B-dyed IP-L 780 photoresist for the first base structures, (*iii*) IP-L 780 for the second base, (*iv*) Methylene Blue-dyed IP-L 780 for the third base, and (*v*) Cy5-dyed IP-L 780 for the last base. After fabrication, we manually removed the PDMS from the glass substrate using forceps (**Fig. 2d**). SEM results of fabricated structures revealed that the majority of the multi-material base pairs printed successfully (*e.g.*, **Fig. 3a**). One caveat, however, is that a small proportion of the designed base pairs lacked the formation of the complementary base (*i.e.*, base 3 and base 4). In addition to the design complexity, a possible basis for such results is the relatively high aspect ratios of the initially printed bases (*i.e.*, approximately 10 to 20), which may contribute to temporary misalignment in response to the microfluidic loading process. Notably, prior microfluidics-based DLW methods have avoided printing microstructures with aspect ratios greater than 1.[29,30]

To investigate the potential role of feature aspect ratio in the efficacy of microfluidic DLW, we also employed μFMM-DLW to print multi-material systems with low-aspect-ratio microstructures. In particular, we fabricated a two-material cello-inspired microstructure comprising Ormocomp photoresist for the base (**Fig. 3b,c** – *grey*; aspect ratio = 0.2) and IP-L 780 photoresist for the neck and bridge (**Fig. 3b,c** – *green*; aspect ratio ≈ 1.0). Confocal fluorescence microscopy results revealed uniquely fluorescent signatures corresponding to the distinct materials as well as the successful integration of the multi-material structures (**Fig. 3c**). In addition, we also printed a four-material 3D structure inspired by the University of Maryland logo, which included: (*i*) non-fluorescent IP-Dip photoresist for the circular base (**Fig. 3d** – *grey*), IP-L 780 photoresist for the checkered section (**Fig. 3d,e** – *yellow*), Rhodamine B-dyed IP-L 780 for the cross bottony (**Fig. 3d,f** – *red*), and Cy5-dyed IP-L 780 for the text (**Fig. 3d,g** – *blue*). Confocal fluorescence microscopy results revealed that the autofluorescence of the IP-L 780 material led to excitation at multiple lower wavelengths (*e.g.*, 405 nm and 480 nm) (**Fig. 3e,g** – *yellow*; *blue*). Such phenomena, however, are unrelated to μFMM-DLW performance, which appeared well suited for low-aspect-ratio multi-material microstructure fabrication (**Fig. 3b-h**).

Previously, researchers have utilized conventional multi-material DLW methods for numerous applications; however, results for the multi-material registration capabilities of these protocols have never been reported in the literature.[33] To establish a baseline with which to compare such approaches to the presented μFMM-DLW strategy, we designed a set of two-material microstructures corresponding to a relatively planar orientation and an angled orientation (∼25°). Both designs included an IP-L 780 base component with alignment features and a Rho-

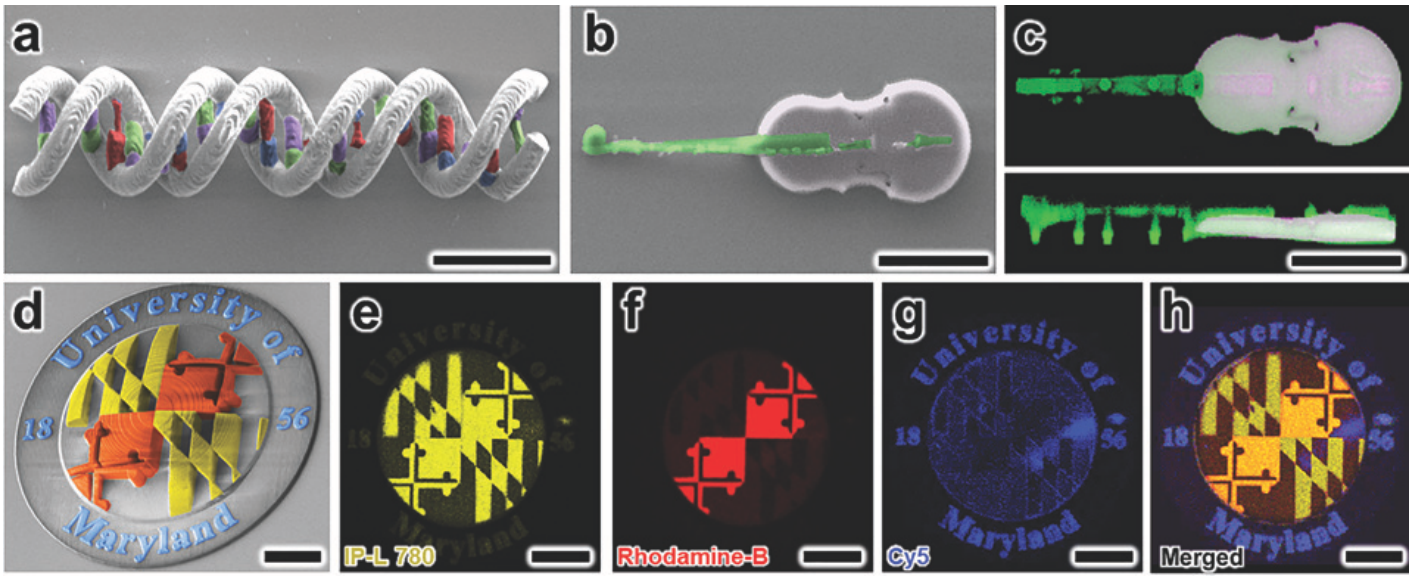

Fig. 3 Results for various multi-material microstructures fabricated *via* μFMM-DLW. (**a**) False-colored SEM results for a five-material DNA-inspired component. *Grey* = IP-Dip; *Red* = Rhodamine B-dyed IP-L 780; *Green* = IP-L 780; *Blue* = Methylene Blue-dyed IP-L 780; *Purple* = Cy5-dyed IP-L 780. (**b, c**) False-colored SEM results (**b**) and confocal fluorescence micrographs (**c**) of a two-material cello-inspired structure. *Grey* = Ormocomp; *Green* = IP-L 780. (**d-h**) False-colored SEM results (**d**) and confocal fluorescence micrographs (**e-h**) of a four-material University of Maryland logo component. Scale bars = (**a**) 10 μm; (**b-h**) 25 μm

damine B-dyed IP-L 780 complementary cross structure, which when printed together, allow for optical characterization of multi-material registration. Initially, three users employed conventional multi-material DLW methods (*see also* **ESI Text**†; **ESI Fig. S1**†; **ESI Movie S2**†) to manufacture the two-component systems (*e.g.*, **Fig. 4a,b**). In addition, we utilized μFMM-DLW to fabricate identical system designs (*e.g.*, **Fig. 4c,d**). Thereafter, we acquired SEM micrographs of both sets of fabrication results for subsequent analysis using the software, ImageJ (NIH, Bethesda, MD, USA).

Experimental results for multi-material registration revealed key differences in alignment capabilities for μFMM-DLW and conventional methods (**Fig. 4e,f**). For the relatively planar two-component systems (*e.g.*, **Fig. 4a,c**), conventional techniques resulted in average registration errors of 710±520 nm (ΔX) and 350±230 nm (ΔY) compared to 120±70 nm (ΔX) and 250±210 nm (ΔY) for μFMM-DLW. We observed a similar trend for the angled designs (*e.g.*, **Fig. 4b,d**), with conventional protocols yielding average registration errors of 860±810 nm (ΔX) and 420±190 nm (ΔY) *versus* 90±80 nm (ΔX) and 120±110 nm (ΔY) for μFMM-DLW. For the conventional methods, the sample mean of the ΔX registration error was slightly larger than the ΔY results for both the planar and angled architectures (p = 0.15 and 0.13, respectively). One potential basis for this result is that the microscope camera utilized for manual alignment (**ESI Movie S2**†) must be positioned at a slight angle, which may render manual alignment difficult in the X direction. The elimination of the manual alignment step likely accounts for the absence of such trends in the μFMM-DLW results, which not only lacked significant differences between ΔX and ΔY errors for both the planar and angled components (p = 0.27 and 0.71, respectively), but also revealed smaller ΔX errors in both cases. Combining the ΔX and ΔY results to obtain the full magnitude of material registration revealed a reduction in error from 930±660 nm to 220±170 nm for the conventional and μFMM-DLW strategies, respectively – a significant improvement in both the accuracy ($p < 0.01$) and precision (as measured by standard deviation) for multi-material alignment.

An additional metric of interest for DLW manufacturing is the overall fabrication and processing time. To elucidate potential differences between μFMM-DLW and conventional DLW, we monitored the time associated with each fabrication step for printing the two-material alignment structures (*e.g.*, **Fig. 4a-d**) for each approach. The results for fabrication time revealed that conventional DLW manufacturing, alignment, and post-processing of the two-material components required 62±9 min, while the μFMM-DLW required 22±1 min – a reduction of approximately 65% (**ESI Fig. S3**†). Notably, these results are for a two-material system (with only one alignment step), and thus, it is likely that for components with higher numbers of distinct integrated materials, the μFMM-DLW will provide additional benefits in terms of reducing the time and labor required for DLW manufacturing.

In this work, we reported a facile multi-material DLW approach that combines standard PDMS micromolding, impermanent PDMS-to-glass bonding, vacuum-based microfluidic loading, and *is*DLW to provide an accessible pathway toward high-resolution 3D manufacturing of multi-material nanostructured components. Compared to conventional multi-material DLW protocols, the presented μFMM-DLW strategy yielded a considerable improvement in the total fabrication and processing time, while simultaneously enhancing both the multi-material registration accuracy and repeatability. In particular, the experimental results revealed an over 75% reduction in the magnitude of the overall registration error ($p < 0.01$) as well as a decrease in the error variation (from a standard deviation of 660 nm to 170 nm). The μFMM-DLW approach also eliminates the need for

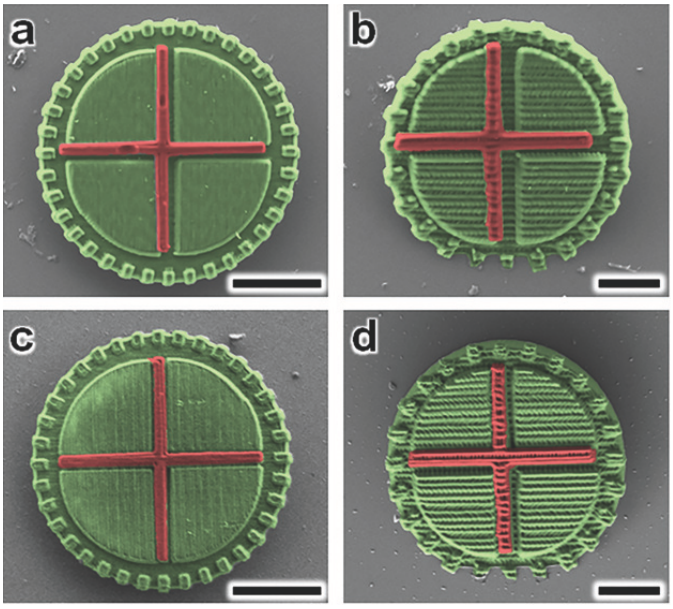

Fig. 4 Experimental multi-material registration results for two-material components fabricated *via* conventional multi-material DLW and μFMM-DLW. (**a-d**) False-colored SEM micrographs of representative (**a,c**) relatively planar and (**b,d**) ~25° angled two-material microstructures corresponding to: (**a,b**) conventional multi-material DLW, and (**c,d**) μFMM-DLW. (**e,f**) Histograms of sample multi-material registration error for all two-material microstructures fabricated using: (**e**) conventional multi-material DLW (n = 15), and (**f**) μFMM-DLW (n = 8). Scale bars = 10 μm

multiple N_2 drying steps associated with conventional development protocols, which offers a possible means to mitigate failure modes stemming from intermediate liquid-to-vapor transitions, such as stiction.[34] In addition, the μFMM-DLW provides a notable expansion of multi-material DLW by supporting *is*DLW[31,32] of multi-material systems. In such cases (which require permanently sealed devices), the PDMS can be permanently bonded to glass substrates (*e.g.*, *via* O_2 plasma treatment) without further consequence to the μFMM-DLW process. One caveat to the presented approach, however, is that the fabrication results revealed a potential role for feature aspect ratio in multi-material printing efficacy, with low-aspect-ratio microstructures corresponding to improved μFMM-DLW performance. As prior reports have involved the printing of features with aspect ratios of approximately 1 or less,[29,30] future works should focus on investigating the challenges associated with manufacturing high-aspect-ratio structures *via* microfluidics-based DLW. Nonetheless, the fabrication and experimental results in this work demonstrate a potential for this strategy to enable new classes of geometrically complex multi-material, and in turn, multi-functional 3D microsystems for fields including optical and mechanical meta-materials, photonics, and cellular research.

Conflicts of Interest

There are no conflicts of interest to declare.

Acknowledgements

The authors greatly appreciate the help and support of Maryland Nanocenter staff including John Abrahams, Jonathan Hummel, Mark Lecates, Thomas Loughran, Dr. Wen-An Chiou, and Dr. Sz-Chian Liou, and members of the Bioinspired Advanced Manufacturing Laboratory and Terrapin Works. This work was supported in part by NSF Award Number 1761395.

References

1 T. Gissibl, S. Thiele, A. Herkommer and H. Giessen, *Nature Communications*, 2016, **7**, 11763.
2 P.-I. Dietrich, M. Blaicher, I. Reuter, M. Billah, T. Hoose, A. Hofmann, C. Caer, R. Dangel, B. Offrein, U. Troppenz, M. Moehrle, W. Freude and C. Koos, *Nature Photonics*, 2018, **12**, 241–247.
3 N. Kedia, Z. Liu, R. D. Sochol, J. Tam, D. X. Hammer and A. Agrawal, *Optics Letters*, 2019, **44**, 1825–1828.
4 T. Ergin, N. Stenger, P. Brenner, J. B. Pendry and M. Wegener, *Science*, 2010, **328**, 337–339.
5 T. Bückmann, M. Thiel, M. Kadic, R. Schittny and M. Wegener, *Nature Communications*, 2014, **5**, 4130.
6 J. Li, X. Li, T. Luo, R. Wang, C. Liu, S. Chen, D. Li, J. Yue, S.-h. Cheng and D. Sun, *Science Robotics*, 2018, **3**, eaat8829.
7 S. Lee, S. Kim, S. Kim, J.-Y. Kim, C. Moon, B. J. Nelson and H. Choi, *Advanced Healthcare Materials*, 2018, **7**, 1700985.
8 F. Kotz, K. Arnold, W. Bauer, D. Schild, N. Keller, K. Sachsenheimer, T. M. Nargang, C. Richter, D. Helmer and B. E. Rapp, *Nature*, 2017, **544**, 337–339.
9 M. R. Gullo, S. Takeuchi and O. Paul, *Advanced Healthcare Materials*, 2017, **6**, 1601053.
10 P. Mueller, M. Thiel and M. Wegener, *Optics Letters*, 2014, **39**, 6847–6850.
11 G. Seniutinas, A. Weber, C. Padeste, I. Sakellari, M. Farsari and C. David, *Microelectronic Engineering*, 2018, **191**, 25–31.
12 A. K. Au, N. Bhattacharjee, L. F. Horowitz, T. C. Chang and A. Folch, *Lab on a Chip*, 2015, **15**, 1934–1941.
13 H. Gong, A. T. Woolley and G. P. Nordin, *Lab on a Chip*, 2016, **16**, 2450–2458.
14 J. R. Tumbleston, D. Shirvanyants, N. Ermoshkin, R. Januszewicz, A. R. Johnson, D. Kelly, K. Chen, R. Pinschmidt, J. P. Rolland, A. Ermoshkin, E. T. Samulski and J. M. DeSimone, *Science*, 2015, **347**, 1349–1352.
15 B. E. Kelly, I. Bhattacharya, H. Heidari, M. Shusteff, C. M. Spadaccini and H. K. Taylor, *Science*, 2019, **363**, 1075–1079.
16 R. D. Sochol, E. Sweet, C. C. Glick, S.-Y. Wu, C. Yang, M. Restaino and L. Lin, *Microelectronic Engineering*, 2018, **189**, 52–68.
17 F. Klein, B. Richter, T. Striebel, C. M. Franz, G. v. Freymann, M. Wegener and M. Bastmeyer, *Advanced Materials*, 2011, **23**, 1341–1345.
18 A. C. Scheiwe, S. C. Frank, T. J. Autenrieth, M. Bastmeyer and M. Wegener, *Biomaterials*, 2015, **44**, 186–194.
19 Y. Da Sie, Y.-C. Li, N.-S. Chang, P. J. Campagnola and S.-J. Chen, *Biomedical Optics Express*, 2015, **6**, 480–490.
20 M. M. Zieger, P. Mueller, A. S. Quick, M. Wegener and C. Barner-Kowollik, *Angewandte Chemie International Edition*, 2017, **56**, 5625–5629.
21 D. Gräfe, A. Wickberg, M. M. Zieger, M. Wegener, E. Blasco and C. Barner-Kowollik, *Nature Communications*, 2018, **9**, 2788.
22 F. Mayer, S. Richter, P. Hübner, T. Jabbour and M. Wegener, *Advanced Materials Technologies*, 2017, **2**, 1700212.
23 M. Schmid, S. Thiele, A. Herkommer and H. Giessen, *Optics Letters*, 2018, **43**, 5837–5840.
24 D. Serien and S. Takeuchi, *ACS Biomaterials Science & Engineering*, 2017, **3**, 487–494.
25 B. Richter, V. Hahn, S. Bertels, T. K. Claus, M. Wegener, G. Delaittre, C. Barner-Kowollik and M. Bastmeyer, *Advanced Materials*, 2017, **29**, 1604342.

26 T. K. Claus, B. Richter, V. Hahn, A. Welle, S. Kayser, M. Wegener, M. Bastmeyer, G. Delaittre and C. Barner-Kowollik, *Angewandte Chemie International Edition*, 2016, **55**, 3817–3822.

27 H. Ceylan, I. C. Yasa and M. Sitti, *Advanced Materials*, 2017, **29**, 1605072.

28 M. Malinauskas, A. Žukauskas, S. Hasegawa, Y. Hayasaki, V. Mizeikis, R. Buividas and S. Juodkazis, *Light: Science & Applications*, 2016, **5**, e16133.

29 A. C. Lamont, M. A. Restaino and R. D. Sochol, Proceedings of the 32nd International Conference on Micro Electro Mechanical Systems, Seoul, South Korea, 2019, pp. 237–240.

30 F. Mayer, S. Richter, J. Westhauser, E. Blasco, C. Barner-Kowollik and M. Wegener, *Science Advances*, 2019, **5**, eaau9160.

31 J. Lölsberg, J. Linkhorst, A. Cinar, A. Jans, A. J. C. Kuehne and M. Wessling, *Lab on a Chip*, 2018, **18**, 1341–1348.

32 A. C. Lamont, A. T. Alsharhan and R. D. Sochol, *Scientific Reports*, 2019, **9**, 394.

33 C. Barner-Kowollik, M. Bastmeyer, E. Blasco, G. Delaittre, P. Mueller, B. Richter and M. Wegener, *Angewandte Chemie International Edition*, 2017, **56**, 15828–15845.

34 B. K. Mousavi, A. K. Mousavi, T. J. Hieber, J. Chen and Z. C. Leseman, *Journal of Micromechanics and Microengineering*, 2019, **29**, 075013.

We present an accessible strategy for printing multi-material 3D nanostructured components via microfluidic two-photon direct laser writing.